Spatial control over near-critical-point operation ensures fidelity of ParAB*S*-mediated bacterial genome segregation

Longhua Hu[1], Jerome Rech[2], Jean-Yves Bouet[2, 3], Jian Liu[1, 3]

1. Department of Cell Biology, Center for Cell Dynamics, Johns Hopkins University School of Medicine, Baltimore, MD 21205, USA;
2. Laboratoire de Microbiologie et Génétique Moléculaires, Centre de Biologie Intégrative (CBI), Centre National de la Recherche Scientifique (CNRS), Université de Toulouse, UPS, F-31000 Toulouse, France;
3. Corresponding Authors: jean-yves.bouet@univ-tlse3.fr (JYB); jliu187@jhmi.edu (JL)

ABSTRACT

In bacteria, most low-copy-number plasmid and chromosomally encoded partition systems belong to the tripartite ParAB*S* partition machinery. ParAB*S* system presents a prototypic model to understand the mechanisms of bacterial genome segregation, which despite its importance in genetic inheritance, are not well understood. Combining theory and experiment, we provided evidences that the ParAB*S* system – partitioning via the ParA gradient-based Brownian ratcheting – operates near a critical point *in vivo*. This near-critical-point operation adapts the segregation distance of replicated plasmids to the half-length of the elongating nucleoid, ensuring both cell halves to inherit one copy of the plasmids. Further, we demonstrated that the plasmid localizes the cytoplasmic ParA to buffer the partition fidelity against the large cell-to-cell fluctuations in ParA level. We suggest that the spatial control over the near-critical-point operation ensures both sensitive adaption and robust execution of partitioning – a basic principle that could shed light on bacterial genome partition.

INTRODUCTION

Cellular processes must establish the right operating point in a very large parameter space – that allows robust execution of biological function and simultaneously sensitive adaptation to environmental cues. What is the character of this right operating point? How do cells find and maintain it? It is postulated that all living systems operate near the edge of phase transition (1), *i.e.*, near a critical point where the system is halfway between two phases in its parameter space. Operating near such a tipping point allows the system to sensitively adapt to changes. While increasing evidences support this notion (2-5), they are largely statistical inference from experimental data and lack the physical mechanisms that give rise to the near-tipping-point behavior. Crucially, it is unclear how cellular processes maintain the robustness of operating near the critical point, in the presence of ever-lasting noises (*e.g.*, the fluctuations in gene expression at a single-cell level (6-8)). From this perspective, we set out to examine the physical mechanism of bacterial DNA segregation with the emphasis on how the operating point of DNA partition machinery is controlled to maximize the partition fidelity. We exploited low-copy-number plasmid partition in bacteria as the model system by combining theoretical modeling with experimental testing.

Segregating replicated genomes before cell division is essential to ensure faithful genetic inheritance. Despite its simple form, partitioning of low-copy-number plasmids in bacteria is robust with an extremely low error rate ($<10^{-4}$ per generation) (9), and provides a tractable paradigm to understand fundamental principles of genome segregation (10). Most low-copy-number plasmids are actively partitioned – by a conserved tripartite ParAB*S* system – along the nucleoid, a rod-like structure consisting primarily of condensed chromosomal DNA. While cargo trafficking *in vivo* typically utilizes cytoskeletal filament or motor protein-based mechanisms, the ParAB*S* machinery utilizes none of the conventional mechanisms for partitioning (11-14). How the ParAB*S* system drives genome partitioning has puzzled the field since its first postulation in the replicon theory (15). The key elements of ParAB*S* system are as follows (10): ParA is an ATPase that binds non-specifically to DNA in nucleoid in an ATP-bound dimeric state. ParB is the adaptor protein. It binds specifically at a centromere-like site *parS* on the plasmid and sequence-nonspecifically around *parS* to form large clusters called partition complexes (PCs). ParB regulates ParA DNA binding by (i) direct interaction that provokes its release from the nucleoid (13), and by (ii) stimulating the ATPase activity that convert ParA in the ADP-bound form that do not bind nucleoid DNA (16,17). It is not understood how the chemical energy provided by ATP hydrolysis is harnessed to ensure the PC partition fidelity, beside its important implication in separating newly duplicated *parS* sites (18).

Spatial-temporal features of the ParAB*S* system expose some clues of its inner-working. PCs move around, and frequently switch directions over the cell length (11,19-23). As the timing of PC replication and segregation is not directly coupled to cell cycle and the nucleoid itself keeps elongating before cell division (24-26), the replicated PCs can be anywhere along the nucleoid length when they start to split apart (22). Intriguingly, the replicated PCs always first move apart persistently and then position themselves with the separation being ~ half of the cell length (11,19,20,22,27). While segregating by half of the cell length ensures the partition fidelity by always positioning the replicated PCs in the different cell halves, it precipitates the following questions. First, given that the PCs locally interact with the nucleoid, which elongates in proportion to the cell length (28), the question becomes: How do the PCs have the global "view" of, and adapt their separation to, the length of the elongating

nucleoid and, ultimately, the half of the cell length? Second, what ensures the partition robustness in the presence of ever-lasting noises, *e.g.*, the fluctuations in protein levels?

We previously established the ParA protein gradient-based Brownian ratchet model – a new mechanism of processive cargo transport, without resorting to filament nor motor proteins (29,30). With multiple ParA-ParB bonds tethering a *parS*-coated cargo to a DNA carpet, ParB-stimulated bond dissociation triggers the release of the ParA from the DNA carpet, the randomness of which results in a force imbalance that drags the cargo forward. Critically, the time delay in resetting ParA DNA-binding affinity generates a ParA-depletion zone behind the forward moving cargo (14,29,31), perpetuating the asymmetry and persistent movement. As such, the ParAB*S* system can work as a Brownian ratchet: the ParB-bound cargo "self-drives" by both creating and following a ParA gradient over the DNA. This protein gradient-based Brownian ratchet model provides a conceptual framework that allowed us to explain – for the first time in a coherent manner – the diverse motility patterns of PCs evidenced *in vivo* (32) and starts to gain support from *in vivo* experiments (33-36). However, our effort so far focused on a highly simplified picture, it is unclear 1) whether and how this Brownian ratchet mechanism can adapt the plasmid segregation distance to the length of an elongating nucleoid, and 2) how the PC partition ensures its fidelity against cellular noises.

Here, we show that 1) this ParA gradient-based Brownian ratcheting of bacterial low-copy-number plasmid partitioning operates near a critical point *in vivo*, and 2) the spatial controls over the near-critical-point operation allow both sensitive adaptation of partition to the nucleoid length and robust execution of partition to buffer against noises.

MATERIALS AND METHODS

Qualitative model description

We first built the *in vivo* model – to specifically capture how ParA-mediated PC partition responds to the dynamical changes – associated with nucleoid elongation during cell growth. The qualitative model features are described below (Figure 1).

Our model begins with two PCs arranged side-by-side to mimic the replicated PCs and examines the subsequent partition dynamics. As a starting point of the modeling, we depict each PC as a circular disc of ~ 100 nm in radius (34,37), the nucleoid as a flat rectangle, and the cytoplasm as a 2D domain of the same dimension as the nucleoid (Figure 1A). To capture the dynamic changes associated with nucleoid elongation and cell growth, the model describes two effects. First, with their widths fixed at 1.0 μm, the nucleoid and cytosolic domains elongate at a constant rate (~ 6-18 nm/min) measured by our experiments (Figure 1B), in which we imaged HU-mCherry-tagged nucleoid over time in *E. coli* growing in minimal growth medium. The initial nucleoid length is set to be 2 μm, if not otherwise mentioned. Second, the model depicts that concurrent with nucleoid elongation, new ParA molecules are generated to keep ParA concentration constant. This captures the essence of observed auto-regulation of ParA expression (38,39) and Western-blot measurements showing the constant ParA concentration on population-level (37).

Accordingly, the model depicts the moving boundary lengthwise and imposes hard-wall boundary condition for ParA and ParB at all edges of the simulation domain. While ParB only localizes to the PCs (37), ParA can exchange between the nucleoid and the cytoplasm in accordance to the reaction-diffusion scheme (Figures 1B, C). Specifically, ParA·ATP binds to

vacant, unoccupied locations of the nucleoid at a basal rate (13,40), and can transiently unbind and rebind to adjacent vacant sites via lateral diffusion (41). Upon binding to plasmid-bound ParB, the ParA·ATP no longer diffuses but forms a ParA·ATP-ParB bond, tethering the PC to the nucleoid through the nucleoid-ParA·ATP-ParB-plasmid linkage. For simplicity we refer the entire linkage as the ParA-ParB bond (Figure 1C).

The ParA-ParB bond formation and the subsequent deformation, similar to deforming a spring, generates a restoring force on the PC (Figure 1C). The vector sum of many individual ParA-ParB bonds across the PC collectively generates a net force that displaces the PC. The movement of PC in turn changes the bond configurations. When random events (*e.g.*, PC diffusion and stochastic ParA-ParB bond dynamics) break symmetry, the PC moves forward with the ParA-ParB bonds broken at its back (Step 1 in Figure 1C).

We define the resulting disengaged ParA to be in a distinctive state, $ParA^D$ (Figure 1B). While the model does not specify whether $ParA^D$ corresponds to an ATP-bound or ADP-bound state, it recapitulates two key aspects of disengaged ParA. First, $ParA^D$ dissociates from the nucleoid faster than the basal turnover rate of ParA·ATP, which reflects the known effect of ParB-mediated stimulation on ParA release from the nucleoid (13,40). Second, once $ParA^D$ dissociates into the cytoplasm, it slowly reverts to the ATP-bound state competent for DNA-binding (13,40). This time delay results in a ParA-depletion zone trailing behind the moving PC, which subsequently can be refilled by cytosolic and nucleoid-associated ParA·ATP.

As the PC moves forward, the ParBs on the leading edge of the PC continue to establish new bonds with ParA·ATP on unexplored regions of the nucleoid, where the ParA·ATP concentration is higher (Step 2 in Figure 1C). PC movement therefore maintains the asymmetric ParA concentration gradient that in turn supports further forward movement (Step 3 in Figure 1C), resulting in a directed and persistent movement. Conceptually, our model is a two-dimensional burnt-bridge Brownian ratchet model (42,43), in which mechanical actions of the multiple bonds not only facilitate the forward cargo movement, but collectively provide tethering that quenches the cargo lateral diffusion. This drives the directed and persistent movement.

Quantitative model formulation and simulation details

To quantitatively elucidate the proposed mechanism, we numerically compute our model with the parameters capturing *in vivo* conditions (Table S1 in Supplemental Data). The nucleoid-bound ParA·ATPs were initially in chemical equilibrium with their cytosolic counterparts and were randomly distributed on the nucleoid lattice with 5 nm spacing. ParBs were permanently distributed with a uniform density of ~ 0.013 ParB dimer/nm^2 over the PC, reflecting the known high propensity of ParB to spreading around the *parS* site on the plasmid (37,44-46). We model each ParA-ParB bond as an elastic spring. The vertical distance between the nucleoid and the PC was fixed at the equilibrium length of ParA-ParB bond (L_e). The stochastic reactions involving PC-bound ParB, nucleoid-bound and cytosolic ParAs are simulated with the kinetic Monte Carlo scheme according to the reaction scheme (Figure 1B).

The simulation workflow is as follows. At each simulation time step, each ParB can interact with available ParA·ATP within a distance L_a, and bind only one ParA at a time with a rate of k_on (Step 1 in Figure 1C). The probability of binding is proportional

to $e^{-\frac{1}{2}\frac{k_s(L-L_e)^2}{k_BT}}$ for $L_a > L > L_e$; otherwise, it is zero. k_s is the spring constant of the bond, L denotes the separation between ParB and ParA·ATP. If this bond forms, L is the instantaneous bond length, $\frac{1}{2}k_s(L-L_e)^2$ represents the associated elastic energy penalty. Importantly, given the model parameters, this energy penalty is less than the thermal energy, k_BT. Consequently, thermal energy is sufficient to pre-stretch the newly formed bond, which in turn provides an elastic force $f = k_s(L-L_e)$ (Step 2 in Figure 1C). In the simulation, we vector-sum the elastic forces from all the ParA-ParB bonds over the PC. This net force together with the PC diffusion drives PC motion for one simulation step (Step 3 in Figure 1C), following the Langevin-like dynamics: $\frac{k_BT}{D_p}\frac{dX_p}{dt} = \sum_i \vec{f_i} + \zeta(t)$. Here, X_p is the centroid position of the PC, D_p is the diffusion constant of the PC, $\vec{f_i}$ is the elastic force from the ith ParA-ParB bond on the PC, and $\zeta(t)$ represents random force resulting from thermal motion of the solvent molecules with $\langle\zeta(t_1)\zeta(t_2)\rangle = \frac{2k_BT}{D_p}\delta(t_1-t_2)$ and $\delta(t_1-t_2)$ is the Dirac delta function.

In the next time step, the lengths and orientations of the ParA-ParB bonds are updated by the PC motion, from which the dissociation rates of the existing ParA-ParB bonds are calculated: when the bond extension exceeds the maximum, X_C (*i.e.*, $(L-L_e) > X_C$), the bond breaks instantaneously; otherwise, the dissociation rate is k_{off}. This dissociation reaction is next implemented in the stochastic simulation. The resulting ParA^D will be released into cytoplasm and convert at a slow rate of k_n ($k_n \ll k_{off}$) to ParA·ATP. Additionally, new ParA·ATPs are generated in cytosol concurrently with the elongation of nucleoid and cytoplasmic domains at the rate of k_{nl}. These ParA·ATPs can bind to the nucleoid with a rate of k_a.

Meanwhile, PC movement from the previous time step permits PC-bound ParBs to explore new territory and form bonds with available ParA·ATPs, and vacancies on the nucleoid can be re-filled by ParA·ATP rebinding from the cytosol or diffusing from adjacent sites on the nucleoid. These ParA·ATPs can establish new bonds with ParB if the PC is nearby. We then update the net force from all the ParA-ParB bonds, including changes in existing bonds and newly formed bonds. The movement of the cargo is then calculated as in the previous time step. We repeat these steps throughout the simulation over time.

Bacterial strains and plasmids

E. coli K-12 strains are derivatives of DLT1215 (47) and transformed with the plasmids pJYB240 (48), pJYB243 (37) or pJYB249 (48). Cultures were grown at 37°C with aeration in LB (49) containing thymine (10 µg.ml-1) and antibiotics as appropriate: chloramphenicol (10 µg.ml^{-1}); kanamycin (50 µg.ml^{-1}). For microscopy assays, cultures were grown at 30°C with aeration in MGlyC (M9 minimal medium supplemented with 0.4 % glycerol, 0.2 % casamino acids, 1 mM $MgSO_4$, 0.1 mM $CaCl_2$, 1 µg.ml^{-1} thiamine, 20 µg.ml^{-1} leucine and 40 µg.ml^{-1} thymine).

Epifluorescence microscopy and analysis

Overnight cultures were inoculated into fresh media at a concentration permitting at least 10 generations of exponential growth and incubated at 30°C to an optical density (OD_{600}) of ~0.25. Samples (0.7 µl) were deposited to the surface of a layer of 1% agarose buffered in M9 solution, as described (50). The cells were imaged at 30°C using an Eclipse TI-E/B wide field epifluorescence microscope with a phase contrast objective (CFI Plan APO LBDA 100X oil

NA1.45) and a Semrock filter YFP (Ex: 500BP24; DM: 520; Em: 542BP27) or FITC (Ex: 482BP35; DM: 506; Em: 536BP40). Images were taken using an Andor Neo SCC-02124 camera with illumination at 80% from a SpectraX source Led (Lumencor) and exposure times of 0.2-1 second. Nis Elements AR software (Nikon) was used for image capture and editing. Image analyses were performed using Image J scripts. Tracking the PC and nucleoid length was done in the MicrobeJ plugin in ImageJ (51,52). It involves finding the cells of interest and tuning the parameters in MicrobeJ to get the data. Specifically, for each identified cell, we recorded the length of the cell, integrated fluorescence of ParA, and the peak positions of ParB fluorescence intensity, which were then used to represent the positions of the partition complexes. We also recorded the fluorescence profile of the nucleoid along the long axis of the cell, from which the nucleoid length of the cell was derived using the full-width-half-height approach. For ParA-PC colocalization analysis, we used a self-developed (CBI) Python-based tool (Distance2MaxProfile: https://imaprocess.pythonanywhere.com/Analymage/detail_projet/20/).

RESULTS

ParABS-mediated PC partition operates near a critical point

We formulated the PC partition problem in the framework of dynamical phase transition, which denotes different PC motility modes as distinct states. We defined the order parameter (ψ) – that depicts and distinguishes different states of PC motility – as the PC's excursion range normalized by half of the nucleoid length. For instance, ψ is ~ 0 for being stationary and approaches ~ 1.0 for pole-to-pole oscillation. Further, we used the PC segregation distance as a proxy to infer the partition fidelity: In line with our previous work (32), the more the PC segregation deviates from the half length of nucleoid, the more likely will the two PCs end up in the same half of the dividing cell, compromising the partition fidelity.

Exploiting agent-based stochastic simulations of our model allows us to calculate the phase diagram of PC segregation motility with an elongating nucleoid (Figure 2A), characterized by two key control parameters – the ParA-ParB bond dissociation rate, k_{off}, and the ParA-nucleoid binding rate, k_a. Our calculation suggested that the ParA gradient-based Brownian-ratcheting could allow the replicated PCs to undergo directed segregation and adapt their segregation distance at ~ 0.5 of the increasing nucleoid length (Figure 2B). This ensures the two PCs to always end up in the different cell halves, maximizing the partition fidelity. Importantly, this partition fidelity requires the ParAB*S* system to operate in a very special parameter regime (*e.g.*, the "•" denoted in Figure 2A), which represents the transition of PC motility from directed segregation to pole-to-pole oscillation. At/near this particular parameter set, the PCs are predicted to still undergo directed motility but with extensive excursions, rather than positioning at a specific landmark nor oscillating perpetually all over the place (Figure 2C). Importantly, the statistical distribution of these excursion distances (*i.e.*, the order parameter ψ) is very broad and highly non-Gaussian (Figure 2D), which are distinctive features of critical dynamics (53).

To test the prediction, we conducted time-lapse epifluorescence microscopy experiments using the well-established low-copy-number F-plasmid partition system in *E. coli* (48). We grew *E. coli* in minimal growth medium and used functional fluorescent Par fusion proteins $ParB_F$-mTq2 and HU-mCherry to label the F plasmid and the nucleoid, respectively (Figure 3A). We measured the nucleoid size along the long cell axis and the distance between two PCs in two-foci cells. Our data showed that the PC segregation distance adapts to 0.5 of

nucleoid length as the nucleoid increased from 1.2 micron to 3.0 microns (Figure 3B). Critically, the PCs indeed undergo extensive excursion (Figure 3C) and display a highly non-Gaussian distribution (Figure 3D), which are telltale signs of criticality, confirming our prediction (Figure 2D).

We interpret the physical nature of this near-critical-point PC partition as follows (Figure 2E): Replicated PCs undergoes directed segregation because of their initial side-by-side arrangement. As they deplete the ParA underneath from the nucleoid, the local nucleoid-bound ParA concentration field becomes asymmetric in the "eyes" of each PC, which sets the directed movement. As the PCs move apart, each PC associates with a ParA-depletion zone, like "a sphere of influence". It takes a while for the depleted ParAs to rebind the nucleoid, which eventually re-establish the symmetric ParA distribution surrounding each of the PCs, thus positioning the PCs. As such, the ParA-ParB bond dissociation confers the PC directed segregation, whereas ParA refilling event hinders it. The balance between these two activities defines the tipping point (*aka* the critical point in parameter space). At this tipping point, the PC's ParA-depletion zones (or spheres of influence) overlap and span the entire nucleoid length. This allows the PCs to "feel" not only the presence of each other but the boundary of the elongating nucleoid.

Together, our results suggest that while the ParA-ParB interaction is local, operation of ParA gradient-based Brownian ratchet mechanism – near a critical point – can provide the PCs a global "view" that allows sensitive adaptation of their segregation distance to the increasing nucleoid length.

ParABS-mediated PC partition is robust against cell-to-cell ParA level variations

Given the sensitive nature of partitioning near a critical point, the next question is: How does the ParAB*S*-mediated partition manage to buffer against fluctuations inside cells, the central topic of control for any biological systems? To begin to characterize the cellular fluctuations relevant to ParAB*S*-mediated partition, we measured the intracellular ParA concentration by coupling ParA to m-Venus fluorescent peptide ($ParA_F$-mVenus) in cells allowing to detect the nucleoid length and PC positioning (as above). The data showed that [ParA] varies from cell to cell over 10 folds in wildtype *E. coli* (Figure 4A). And yet, the PC partition still adapts the separation distance to ~ 0.5 of various nucleoid lengths (Figure 4A), ensuring the partition fidelity.

To understand the robustness measure adopted by the PC partition system, we reasoned that both the ParA-ParB dissociation rate, k_{off}, and the ParA-nucleoid binding rate, k_a might change with the [ParA]. This way, the partition could still operate near the criticality when [ParA] varies; i.e., rather than at a fixed point in the parameter space in Figure 2A, the partition operates along the critical line between the states of pole-to-pole oscillation and directed segregation. To explore this possibility, we tried to measure the $ParA_F$-$ParB_F$ dissociation rate k_{off} by monitoring the PC foci segregation rates. According to our model, the PC segregation speed is proportional to the $ParA_F$-$ParB_F$ bond dissociation rate (32). Our data show that the PC segregation speed, although varying somewhat, is insensitive to the [ParA] (Figure 4B). Strikingly, this indicates that the k_{off} and hence, the k_a does not change much under these conditions. However, our current model showed that fixing the parameter set near the critical point, [ParA] variations would significantly perturb the adaptation of segregation distance to nucleoid length (Figure 4C). This cannot be rescued by varying the values of k_{off} and k_a to the similar levels displayed in Figure 4B (data not shown). This discrepancy

suggests partition robustness entails additional factor(s) and thus precipitates the question of what buffers the robustness of PC segregation against [ParA] variations.

PC-mediated ParA localization underlies partition robustness against bulk [ParA] variations

Based on *in vitro* and *in vivo* data suggesting that the ParA binds to ns-DNA and hence could bind to the plasmid DNA (11,13,16), our leading hypothesis is that the intracellular ParA could localize around the PC and create a local environment that buffers the partitioning against the bulk [ParA] variation (Figure 5A). To test the hypothesis, we first extended the current *in vivo* model to incorporate this PC-mediated ParA localization effect. We assumed the cytosolic ParA to have a high binding affinity to PC but with a transient lifetime before turning over into cytoplasm (Figure 5A), characterized by the $k_{\mathrm{on}}^{\mathrm{PC}}$ and k_{off}^{PC} rates. Due to the finite size of the PC, the model imposed an upper limit in the number of ParA molecules ~ 100's that simultaneously localize to the PC. This saturation level is based on the *in vitro* measurements (13,31). We further assumed that right after releasing from the PC, the ParA has a reduced propensity to bind to the nucleoid. This last assumption is based on the observation that the interaction with ParB not only speeds up the dissociation of ParA from nucleoid but inhibits the ParA-nucleoid binding (13). Below, we will present the typical model result, the essence of which persists in a broad range of model parameter space (Figure S1).

Equipped with this ParA localization effect, simulating this integrated mathematical model could explain the robustness of partitioning at the critical point evidenced in *E. coli.* (Figure 4A). That is, the segregation of the replicated PCs by the half of the nucleoid length remains largely insensitive to the [ParA] variations (Figure 5B). This buffering effect entails an appropriate ParA accumulation around the PC (Figure 5C). When the on rate (k_{on}^{PC}) is too slow, the PC not only depletes the ParA from underneath but cannot supply enough ParA to refill the depletion zone underneath so that the PC becomes diffusive (the lower portion of Figure 5C). When the on rate is too fast and the off rate is too slow, the PC will accumulate too many ParAs so that the nucleoid-bound ParA will become very sparse, likewise favoring diffusive movement (the upper left corner of Figure 5C). However, as the off rate increases while keeping the on rate very fast, the PC will funnel the cytoplasmic ParA to the local nucleoid at very high concentration. This significantly increases the overall ParA binding to nucleoid, immobilizing the PCs (the upper right corner of Figure 5C). In these extreme limits, the partition system loses its robustness of adapting the PC segregation distance to the half of an elongating nucleoid (Figure 5C). As such, the ParA needs to localize around the PCs with only several-fold accumulation at its peak concentration to ensure the PC partition fidelity.

To begin to test this prediction of our ParA localization model, we resorted to live-cell imaging to discern the spatial profiles of ParA. We focused our analyses on the new-born cells that have inherited a low amount of $ParA_F$-mVenus – due to the asymmetric ParA distribution at cell division (Figure S2A) – which allows for a better detection of faint localized signal. In these cells with low intracellular amount of ParA, we also imaged the PC locations with $ParB_F$-mTq2 that form intense foci. Although ParA-mVenus displays faint foci, they appeared very close to PCs; importantly, they did not result from cross-fluorescence imaging (Figure S2B). We measured the peak intensity along the cell length for both ParA and ParB by applying a line scan analysis. Figure 5D(i) presents a representative measurement and Figure S2C provides more detailed analysis. Briefly, in the 58 cells analyzed, we observed that the vast majority of them (41 cells) display the same number of

ParA and ParB foci, 14 cells display one more ParA focus than ParB, and 3 cells have one more ParB focus than ParA. However, we could not accurately measure the ParA intensity accumulation around PC because of (i) the cell to cell variation in [ParA] and (ii) the depletion of ParA provoked by ParB. Nevertheless, the observation of discrete ParA patches indicates that ParA accumulates several folds compare to the intracellular level in the close vicinity of PCs, consistent with our predictions (Figure 5D(ii)). To further quantify the level of co-localization of the ParA and ParB foci, we measured the distance between the peak intensities for each pair of ParA and ParB foci (n = 119; Figure 5E). We found that for 98% of the pairs, the ParA and ParB peak intensities are within 2 pixels (131 nm). Given the 200-250 nm resolution of epifluorescence microscopy due to light diffraction limit, our data show that ParA and ParB foci are highly co-localized, providing strong support to the predicted PC-ParA co-localization. Together, our data suggest that PC-mediated ParA localization underlies the robustness of PC partitioning against [ParA] variations.

DISCUSSION

In this paper, we provided direct experimental evidences – with mechanistic understanding – that the partitioning of low-copy-number plasmids operates near a critical point. The near-critical-point operation allows the partition machinery to gauge the size of the entire nucleoid and accordingly, adapt the plasmid segregation distance to the half of the elongating nucleoid (Figure 3). Segregating by half of the nucleoid length renders that each cell halves always inherit at least one PC, ensuring the partition fidelity, which is also observed in other ParABS systems (e.g., (54)). We further provided the data suggesting that the PC localizes cytoplasmic ParA to its neighborhood, creating a local environment that buffers the near-critical-point partition against the fluctuations in bulk [ParA] (Figure 5). We suggest that this spatial control over criticality allows the cell to manage the dichotomy of sensitive adaption and robust execution of low-copy-number plasmid partitioning. This way, each PC "self-drives" by generating the path ahead and erasing the trail behind.

The current model only focuses on the simplest scheme of ParA-PC localization effects. The transient nature in the biochemical interaction between the cytoplasmic ParA and PC, although indicated in experiments (13), remains to be characterized in the future. For instance, the recent findings that ParB binds CTP (55,56) and that *parS*-mediated CTP hydrolysis stimulates ParA interaction (56) open interesting molecular clue to control this interaction. Moreover, our model describes the PC partitioning along the nucleoid surface as a 2D problem. Recent experiments, however, suggest that the PC may move inside the nucleoid (34). This more complicated scenario will be explored in our future effort. Furthermore, this PC-mediated ParA localization effect has its own limitation in ensuring the partition fidelity (Figure S1). For instance, when the nucleoid becomes too long (Figure S1D), the current model would predict the partition machinery to lose its ability of adapting the segregation distance to half of the nucleoid length. Interestingly, as the nucleoid gets longer, the low-copy plasmids are reported to replicate accordingly to keep the plasmid-chromosome ratio constant. The latter events increase the number of PC foci. This way, each PC focus "command" a unitary length of nucleoid as its power of sphere, resulting in the equi-distant pattern (22,57): the two PCs on the same nucleoid segregate by 1/2 of the nucleoid length, whereas the three PCs will segregate by ~ 1/3 of the nucleoid length, and so on. There emerges a size-scaling between the PC inter-distant and the nucleoid length, as a function of PC foci numbers. While the notations of size-scaling and size-control has indicated in biological systems (58-62), our work here provides a functional perspective, in a way similar to spindle-cell size scaling (63). Lastly, because low-copy-number plasmids provide selective advantages for bacterial

survival, connecting the physical mechanism with the fidelity of DNA partition could allow us to understand how evolution shapes the near-critical-point behavior of a biological process to maximize its function. In particular, the ParAB*S*-mediated partition mechanism is widely conserved not only in genome segregation (i.e., plasmids and chromosomes), but also in subcellular organelle trafficking in bacteria (64,65), and yet, it displays distinct spatial-temporal features in different systems (12,66-68). With these diverse spatial-temporal dynamics, our work provides a starting point to shed light on how the near-critical-point operation of the same machinery adapts to different cellular milieus in evolution. We will further investigate in this direction in the near future.

ACKNOWLEDGEMENTS

The authors thanks Drs. Keir Neuman and Kiyoshi Mizuuchi for the inspiring critiques of the work, and Christian Rouvière (ImageAnalysis-CBI) for implementing a python-based analysis tool for colocalization measurements.

FUNDING

L.H.H and J. L. are supported by Johns Hopkins University Startup Funds and Catalyst Awards. J.R and J.Y.B. are supported by an AO80Prime (CNRS) grant.
Conflict of interest statement. None declared.

FIGURE CAPTIONS

Figure 1. Model description. (A) Model setup. (B) Biochemical scheme of ParABS system. (C) Mechanochemical coupling of ParA-ParB bond formation and dissociation underlies ParA gradient-based Brownian ratcheting. The model parameters are listed in Section I in the supplemental information.

Figure 2. Predicted criticality of ParA-mediated PC partition. (A) Predicted phase diagram of PC motility controlled by (k_a, k_{off}). For each point in the phase diagram, we ran stochastic simulations for ≥ 36 trajectories of 10 min-dynamical evolution of the system, starting from the same initial condition and parameter set. The segregation distance reports the average value of ≥ 36 trajectories at the end of the simulation. Here, the ParA concentration is kept constant as ~ 3500 molecules per micron of nucleoid length and other parameters are kept fixed (see Table S1 for details). (B) Segregation distance adapts to 1/2 of the nucleoid length at the critical point in the parameter space. (C) Predicted characteristics of critical point. Left: Order parameter (i.e., the excursion distance of PC) increases continuously as the ParA refilling rate decreases, whereas the variance of the order parameter peaks around the critical point (k_a^*). Right: Corresponding representative simulation trajectory of PC excursion with the parameter set around this critical point. (D) Predicted statistical distribution of PC excursions near the critical point (n=128). (E) Schematic illustration of the physical nature of near-critical-point partitioning.

Figure 3. Critical-point-operation of ParA-mediated PC partition. (A) Experimental setup of two-color live-cell imaging of F-plasmids in wild-type *E. coli*. Cells are observed in phase contrast (top left) and in the blue (top right) and red (bottom right) channels for fluorescence microcopy to observe $ParB_F$-mTq2 or $ParA_F$-mVenus, respectively. Overlay of blue and red channel (bottom left). Cells were grown at 30°C in MGlyC. Scale bar (2 μm). (B) Experimental data demonstrate that PC segregation distance adapts to 1/2 of the nucleoid lengths (n=58). (C) A representative saltatory trajectory of PC excursion. (D) Non-Gaussian distribution of PC excursion distance (n=120).

Figure 4. Robustness of PC partition against variations of ParA level. (A) Experimental data showing the PC segregation distance normalized by the nucleoid length is insensitive to the large cell-to-cell ParA level fluctuations (n=58). (B) Initial segregation speed is insensitive to the ParA level. (C) Current model cannot buffer the near-critical-point partition against ParA level fluctuations.

Figure 5. PC-localization of ParA explains the partition robustness. (A) Model scheme of PC-mediated ParA localization. (B) The amended model can ensure the fidelity of near-critical-point partition against the ParA level fluctuations. (C) Predicted phase diagram of the dependence of PC partition fidelity on the ParA localization effects. For each point in the phase diagram, we ran stochastic simulations for ≥ 36 trajectories of 10 min-dynamical evolution of the system, starting from the same initial condition and parameter set. The segregation distance reports the average value of ≥ 36 trajectories at the end of the simulation. (D) Representative spatial profiles of ParA and PC along the cell length. (i): Live-cell experimental result. Line scan analysis of the fluorescence intensities in arbitrary unit (A.U.) along cell length. Blue and orange lines correspond to the blue ($ParB_F$-mTq2) and yellow ($ParA_F$-mVenus) channels, respectively. The corresponding cell images is displayed in the graph with scale bar (1 μm). The grey area corresponds to 4 pixels (262 nm) around the PC peak. (ii): Model result. (E) Histogram of PC-ParA colocalization.

Reference

1. Mora, T. and Bialek, W. (2011) Are Biological Systems Poised at Criticality? *Journal of Statistical Physics*, **144**, 268-302.
2. Hesse, J. and Gross, T. (2014) Self-organized criticality as a fundamental property of neural systems. *Frontiers in Systems Neuroscience*, **8**.
3. Krotov, D., Dubuis, J.O., Gregor, T. and Bialek, W. (2014) Morphogenesis at criticality. *Proceedings of the National Academy of Sciences*, **111**, 3683-3688.
4. Mojtahedi, M., Skupin, A., Zhou, J., Castaño, I.G., Leong-Quong, R.Y.Y., Chang, H., Trachana, K., Giuliani, A. and Huang, S. (2016) Cell Fate Decision as High-Dimensional Critical State Transition. *PLOS Biology*, **14**, e2000640.
5. Tetzlaff, C., Okujeni, S., Egert, U., Wörgötter, F. and Butz, M. (2010) Self-Organized Criticality in Developing Neuronal Networks. *PLOS Computational Biology*, **6**, e1001013.
6. Elowitz, M.B., Levine, A.J., Siggia, E.D. and Swain, P.S. (2002) Stochastic Gene Expression in a Single Cell. *Science*, **297**, 1183-1186.
7. Kærn, M., Elston, T.C., Blake, W.J. and Collins, J.J. (2005) Stochasticity in gene expression: from theories to phenotypes. *Nature Reviews Genetics*, **6**, 451-464.
8. Newman, J.R.S., Ghaemmaghami, S., Ihmels, J., Breslow, D.K., Noble, M., DeRisi, J.L. and Weissman, J.S. (2006) Single-cell proteomic analysis of S. cerevisiae reveals the architecture of biological noise. *Nature*, **441**, 840-846.
9. Nordström, K. and Austin, S.J. (1989) Mechanisms that contribute to the stable segregation of plasmids. *Annual Review of Genetics*, **23**, 37-69.
10. Bouet, J.-Y. and Funnell, B. (2019) Plasmid Localization and Partition in Enterobacteriaceae. *EcoSal Plus*.
11. Hatano, T. and Niki, H. (2010) Partitioning of P1 plasmids by gradual distribution of the ATPase ParA. *Molecular Microbiology*, **78**, 1182-1198.
12. Lim, H.C., Surovtsev, I.V., Beltran, B.G., Huang, F., Bewersdorf, J. and Jacobs-Wagner, C. (2014) Evidence for a DNA-relay mechanism in ParABS-mediated chromosome segregation. *eLife*, **3**, e02758.
13. Vecchiarelli, A.G., Hwang, L.C. and Mizuuchi, K. (2013) Cell-free study of F plasmid partition provides evidence for cargo transport by a diffusion-ratchet mechanism. *Proceedings of the National Academy of Sciences*, **110**, E1390-E1397.
14. Vecchiarelli, A.G., Neuman, K.C. and Mizuuchi, K. (2014) A propagating ATPase gradient drives transport of surface-confined cellular cargo. *Proceedings of the National Academy of Sciences*, **111**, 4880-4885.
15. Jacob, F., Brenner, S. and Cuzin, F. (1963) On the Regulation of DNA Replication in Bacteria. *Cold Spring Harbor Symposia on Quantitative Biology*, **28**, 329-348.
16. Bouet, J.-Y., Ah-Seng, Y., Benmeradi, N. and Lane, D. (2007) Polymerization of SopA partition ATPase: regulation by DNA binding and SopB. *Molecular Microbiology*, **63**, 468-481.
17. Leonard, T.A., Butler, P.J. and Löwe, J. (2005) Bacterial chromosome segregation: structure and DNA binding of the Soj dimer — a conserved biological switch. *The EMBO Journal*, **24**, 270-282.
18. Ah-Seng, Y., Rech, J., Lane, D. and Bouet, J.-Y. (2013) Defining the Role of ATP Hydrolysis in Mitotic Segregation of Bacterial Plasmids. *PLOS Genetics*, **9**, e1003956.
19. Gordon, S., Rech, J., Lane, D. and Wright, A. (2004) Kinetics of plasmid segregation in Escherichia coli. *Molecular Microbiology*, **51**, 461-469.
20. Niki, H. and Hiraga, S. (1997) Subcellular Distribution of Actively Partitioning F Plasmid during the Cell Division Cycle in E. coli. *Cell*, **90**, 951-957.

21. Ringgaard, S., van Zon, J., Howard, M. and Gerdes, K. (2009) Movement and equipositioning of plasmids by ParA filament disassembly. *Proceedings of the National Academy of Sciences*, **106**, 19369-19374.
22. Sengupta, M., Nielsen, H.J., Youngren, B. and Austin, S. (2010) P1 Plasmid Segregation: Accurate Redistribution by Dynamic Plasmid Pairing and Separation. *Journal of Bacteriology*, **192**, 1175-1183.
23. Walter, J.C., Dorignac, J., Lorman, V., Rech, J., Bouet, J.Y., Nollmann, M., Palmeri, J., Parmeggiani, A. and Geniet, F. (2017) Surfing on Protein Waves: Proteophoresis as a Mechanism for Bacterial Genome Partitioning. *Physical Review Letters*, **119**, 028101.
24. Ellasson, Å., Bernander, R. and Nordström, K. (1996) Random initiation of replication of plasmids P1 and F (oriS) when integrated into the Escherichia coli chromosome. *Molecular Microbiology*, **20**, 1025-1032.
25. Helmstetter, C.E., Thornton, M., Zhou, P., Bogan, J.A., Leonard, A.C. and Grimwade, J.E. (1997) Replication and segregation of a miniF plasmid during the division cycle of Escherichia coli. *Journal of Bacteriology*, **179**, 1393-1399.
26. Onogi, T., Miki, T. and Hiraga, S. (2002) Behavior of Sister Copies of Mini-F Plasmid after Synchronized Plasmid Replication in Escherichia coli Cells. *Journal of Bacteriology*, **184**, 3142-3145.
27. Niki, H. and Hiraga, S. (1999) Subcellular localization of plasmids containing the oriC region of the Escherichia coli chromosome, with or without the sopABC partitioning system. *Molecular Microbiology*, **34**, 498-503.
28. Bakshi, S., Choi, H., Rangarajan, N., Barns, K.J., Bratton, B.P. and Weisshaar, J.C. (2014) Nonperturbative Imaging of Nucleoid Morphology in Live Bacterial Cells during an Antimicrobial Peptide Attack. *Applied and Environmental Microbiology*, **80**, 4977-4986.
29. Hu, L., Vecchiarelli, A.G., Mizuuchi, K., Neuman, K.C. and Liu, J. (2015) Directed and persistent movement arises from mechanochemistry of the ParA/ParB system. *Proceedings of the National Academy of Sciences*, **112**, E7055-E7064.
30. Hu, L., Vecchiarelli, A.G., Mizuuchi, K., Neuman, K.C. and Liu, J. (2017) Brownian ratchet mechanisms of ParA-mediated partitioning. *Plasmid*, **92**, 12-16.
31. Hwang, L.C., Vecchiarelli, A.G., Han, Y.W., Mizuuchi, M., Harada, Y., Funnell, B.E. and Mizuuchi, K. (2013) ParA-mediated plasmid partition driven by protein pattern self-organization. *The EMBO Journal*, **32**, 1238-1249.
32. Hu, L., Vecchiarelli, A.G., Mizuuchi, K., Neuman, K.C. and Liu, J. (2017) Brownian Ratchet Mechanism for Faithful Segregation of Low-Copy-Number Plasmids. *Biophysical Journal*, **112**, 1489-1502.
33. Debaugny, R.E., Sanchez, A., Rech, J., Labourdette, D., Dorignac, J., Geniet, F., Palmeri, J., Parmeggiani, A., Boudsocq, F., Anton Leberre, V. *et al.* (2018) A conserved mechanism drives partition complex assembly on bacterial chromosomes and plasmids. *Molecular Systems Biology*, **14**, e8516.
34. Le Gall, A., Cattoni, D.I., Guilhas, B., Mathieu-Demazière, C., Oudjedi, L., Fiche, J.-B., Rech, J., Abrahamsson, S., Murray, H., Bouet, J.-Y. *et al.* (2016) Bacterial partition complexes segregate within the volume of the nucleoid. *Nature Communications*, **7**, 12107.
35. Schumacher, D., Bergeler, S., Harms, A., Vonck, J., Huneke-Vogt, S., Frey, E. and Søgaard-Andersen, L. (2017) The PomXYZ Proteins Self-Organize on the Bacterial Nucleoid to Stimulate Cell Division. *Developmental Cell*, **41**, 299-314.e213.

36. Uhía, I., Priestman, M., Joyce, G., Krishnan, N., Shahrezaei, V. and Robertson, B.D. (2018) Analysis of ParAB dynamics in mycobacteria shows active movement of ParB and differential inheritance of ParA. *PLOS ONE*, **13**, e0199316.
37. Sanchez, A., Cattoni, Diego I., Walter, J.-C., Rech, J., Parmeggiani, A., Nollmann, M. and Bouet, J.-Y. (2015) Stochastic Self-Assembly of ParB Proteins Builds the Bacterial DNA Segregation Apparatus. *Cell Systems*, **1**, 163-173.
38. Mori, H., Mori, Y., Ichinose, C., Niki, H., Ogura, T., Kato, A. and Hiraga, S. (1989) Purification and characterization of SopA and SopB proteins essential for F plasmid partitioning. *Journal of Biological Chemistry*, **264**, 15535-15541.
39. Yates, P., Lane, D. and Biek, D.P. (1999) The F plasmid centromere, sopC, is required for full repression of the sopAB operon. *Journal of Molecular Biology*, **290**, 627-638.
40. Vecchiarelli, A.G., Han, Y.-W., Tan, X., Mizuuchi, M., Ghirlando, R., Biertümpfel, C., Funnell, B.E. and Mizuuchi, K. (2010) ATP control of dynamic P1 ParA–DNA interactions: a key role for the nucleoid in plasmid partition. *Molecular Microbiology*, **78**, 78-91.
41. Surovtsev, Ivan V., Lim, Hoong C. and Jacobs-Wagner, C. (2016) The Slow Mobility of the ParA Partitioning Protein Underlies Its Steady-State Patterning in Caulobacter. *Biophysical Journal*, **110**, 2790-2799.
42. Morozov, A.Y. and Kolomeisky, A.B. (2007) Transport of molecular motor dimers in burnt-bridge models. *Journal of Statistical Mechanics: Theory and Experiment*, **2007**, P12008-P12008.
43. Saffarian, S., Qian, H., Collier, I., Elson, E. and Goldberg, G. (2006) Powering a burnt bridges Brownian ratchet: A model for an extracellular motor driven by proteolysis of collagen. *Physical Review E*, **73**, 041909.
44. Graham, T.G.W., Wang, X., Song, D., Etson, C.M., van Oijen, A.M., Rudner, D.Z. and Loparo, J.J. (2014) ParB spreading requires DNA bridging. *Genes & Development*, **28**, 1228-1238.
45. Rodionov, O., Łobocka, M. and Yarmolinsky, M. (1999) Silencing of Genes Flanking the P1 Plasmid Centromere. *Science*, **283**, 546-549.
46. Lynch, A.S. and Wang, J.C. (1995) SopB protein-mediated silencing of genes linked to the sopC locus of Escherichia coli F plasmid. *Proceedings of the National Academy of Sciences*, **92**, 1896-1900.
47. Bouet, J.-Y., Bouvier, M. and Lane, D. (2006) Concerted action of plasmid maintenance functions: partition complexes create a requirement for dimer resolution. *Molecular Microbiology*, **62**, 1447-1459.
48. Guilhas, B., Walter, J.C., Rech, J., David, G., Walliser, N.-O., Palmeri, J., Mathieu-Demaziere, C., Parmeggiani, A., Bouet, J.Y., Gall, A.L. *et al.* (2019) ATP-driven separation of liquid phase condensates in bacteria. *bioRxiv*, 791368.
49. Miller, J.H. (1972) *Experiments in molecular genetics*. Cold Spring Harbor Laboratory, Cold Spring Harbor, NY.
50. Diaz, R., Rech, J. and Bouet, J.-Y. (2015) Imaging centromere-based incompatibilities: Insights into the mechanism of incompatibility mediated by low-copy number plasmids. *Plasmid*, **80**, 54-62.
51. Schindelin, J., Arganda-Carreras, I., Frise, E., Kaynig, V., Longair, M., Pietzsch, T., Preibisch, S., Rueden, C., Saalfeld, S., Schmid, B. *et al.* (2012) Fiji: an open-source platform for biological-image analysis. *Nature Methods*, **9**, 676-682.
52. Ducret, A., Quardokus, E.M. and Brun, Y.V. (2016) MicrobeJ, a tool for high throughput bacterial cell detection and quantitative analysis. *Nature Microbiology*, **1**, 16077.

53. Goldenfeld, N. (1992) *Lectures On Phase Transitions And The Renormalization Group*. 1st Edition ed. Addison-Wesley, Boca Raton.
54. Ietswaart, R., Szardenings, F., Gerdes, K. and Howard, M. (2014) Competing ParA Structures Space Bacterial Plasmids Equally over the Nucleoid. *PLOS Computational Biology*, **10**, e1004009.
55. Soh, Y.-M., Davidson, I.F., Zamuner, S., Basquin, J., Bock, F.P., Taschner, M., Veening, J.-W., De Los Rios, P., Peters, J.-M. and Gruber, S. (2019) Self-organization of parS centromeres by the ParB CTP hydrolase. *Science*, **366**, 1129-1133.
56. Osorio-Valeriano, M., Altegoer, F., Steinchen, W., Urban, S., Liu, Y., Bange, G. and Thanbichler, M. (2019) ParB-type DNA Segregation Proteins Are CTP-Dependent Molecular Switches. *Cell*, **179**, 1512-1524.e1515.
57. Ebersbach, G., Ringgaard, S., Møller-Jensen, J., Wang, Q., Sherratt, D.J. and Gerdes, K. (2006) Regular cellular distribution of plasmids by oscillating and filament-forming ParA ATPase of plasmid pB171. *Molecular Microbiology*, **61**, 1428-1442.
58. Crowder, Marina E., Strzelecka, M., Wilbur, Jeremy D., Good, Matthew C., von Dassow, G. and Heald, R. (2015) A Comparative Analysis of Spindle Morphometrics across Metazoans. *Current Biology*, **25**, 1542-1550.
59. West, G.B. and Brown, J.H. (2005) The origin of allometric scaling laws in biology from genomes to ecosystems: towards a quantitative unifying theory of biological structure and organization. *Journal of Experimental Biology*, **208**, 1575-1592.
60. Chan, Y.-H.M. and Marshall, W.F. (2012) How Cells Know the Size of Their Organelles. *Science*, **337**, 1186-1189.
61. Willis, L. and Huang, K.C. (2017) Sizing up the bacterial cell cycle. *Nature Reviews Microbiology*, **15**, 606-620.
62. Si, F., Le Treut, G., Sauls, J.T., Vadia, S., Levin, P.A. and Jun, S. (2019) Mechanistic Origin of Cell-Size Control and Homeostasis in Bacteria. *Current Biology*, **29**, 1760-1770.e1767.
63. Chen, J. and Liu, J. (2016) Spindle Size Scaling Contributes to Robust Silencing of Mitotic Spindle Assembly Checkpoint. *Biophysical Journal*, **111**, 1064-1077.
64. MacCready, J.S., Hakim, P., Young, E.J., Hu, L., Liu, J., Osteryoung, K.W., Vecchiarelli, A.G. and Ducat, D.C. (2018) Protein gradients on the nucleoid position the carbon-fixing organelles of cyanobacteria. *eLife*, **7**, e39723.
65. Vecchiarelli, A.G., Mizuuchi, K. and Funnell, B.E. (2012) Surfing biological surfaces: exploiting the nucleoid for partition and transport in bacteria. *Molecular Microbiology*, **86**, 513-523.
66. Fogel, M.A. and Waldor, M.K. (2006) A dynamic, mitotic-like mechanism for bacterial chromosome segregation. *Genes & Development*, **20**, 3269-3282.
67. Marston, A.L. and Errington, J. (1999) Dynamic Movement of the ParA-like Soj Protein of B. subtilis and Its Dual Role in Nucleoid Organization and Developmental Regulation. *Molecular Cell*, **4**, 673-682.
68. Schofield, W.B., Lim, H.C. and Jacobs-Wagner, C. (2010) Cell cycle coordination and regulation of bacterial chromosome segregation dynamics by polarly localized proteins. *The EMBO Journal*, **29**, 3068-3081.

Figure 1.

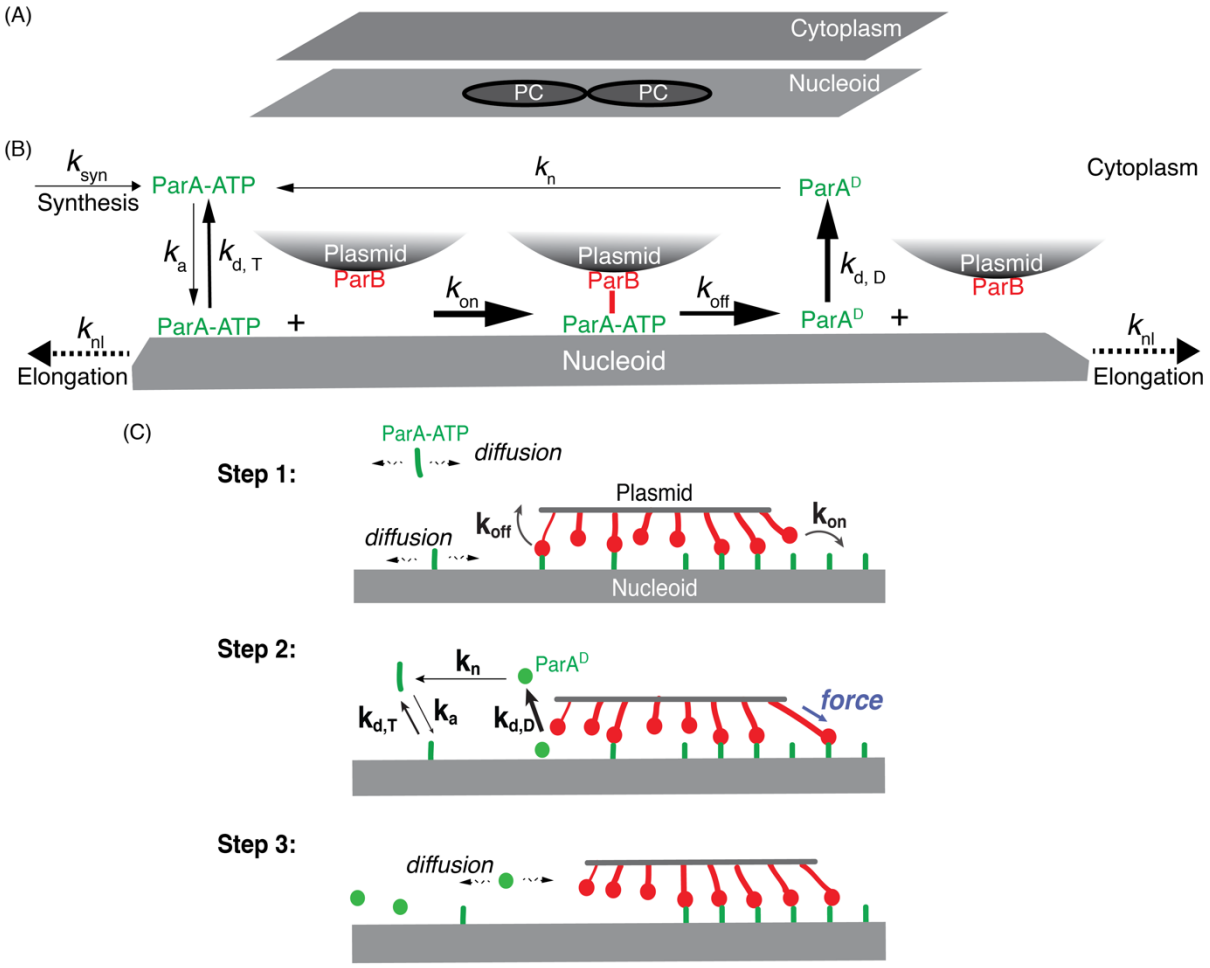
(A)
Cytoplasm
Nucleoid
PC
PC
(B)
k_{syn}
Synthesis
ParA-ATP
k_n
ParA^D
Cytoplasm
k_a
$k_{d,T}$
Plasmid
ParB
k_{on}
k_{off}
$k_{d,D}$
k_{nl}
Elongation
Nucleoid
(C)
Step 1:
ParA-ATP
diffusion
Plasmid
k_{off}
k_{on}
Nucleoid
Step 2:
k_n
ParA^D
$k_{d,T}$
k_a
$k_{d,D}$
force
Step 3:
diffusion

Figure 2.

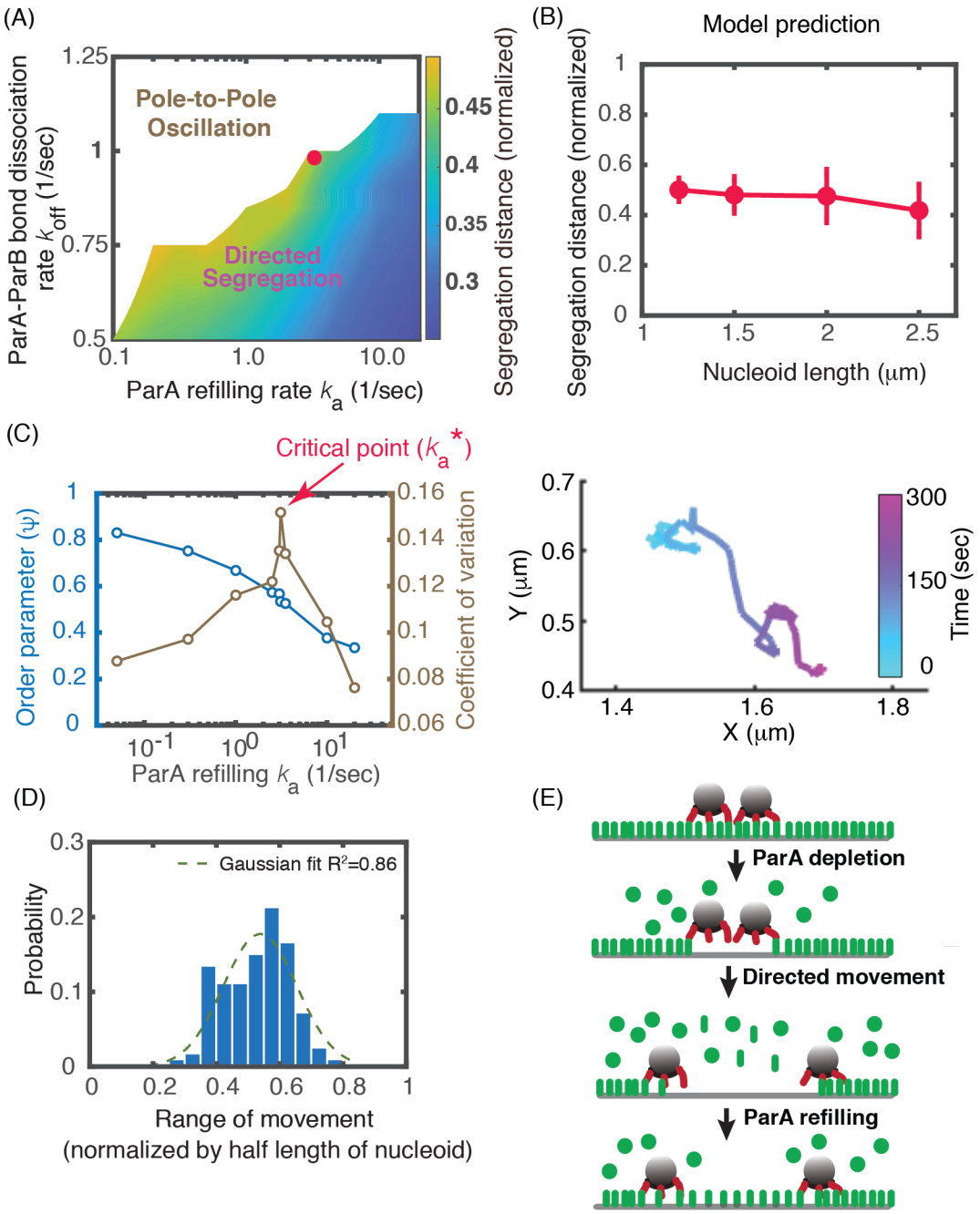
(A)
Pole-to-Pole Oscillation
Directed Segregation
ParA-ParB bond dissociation rate k_{off} (1/sec)
ParA refilling rate k_a (1/sec)
Segregation distance (normalized)
(B)
Model prediction
Segregation distance (normalized)
Nucleoid length (μm)
(C)
Critical point (k_a*)
Order parameter (ψ)
Coefficient of variation
ParA refilling k_a (1/sec)
Y (μm)
X (μm)
Time (sec)
(D)
Gaussian fit R^2=0.86
Probability
Range of movement
(normalized by half length of nucleoid)
(E)
ParA depletion
Directed movement
ParA refilling

Figure 3.

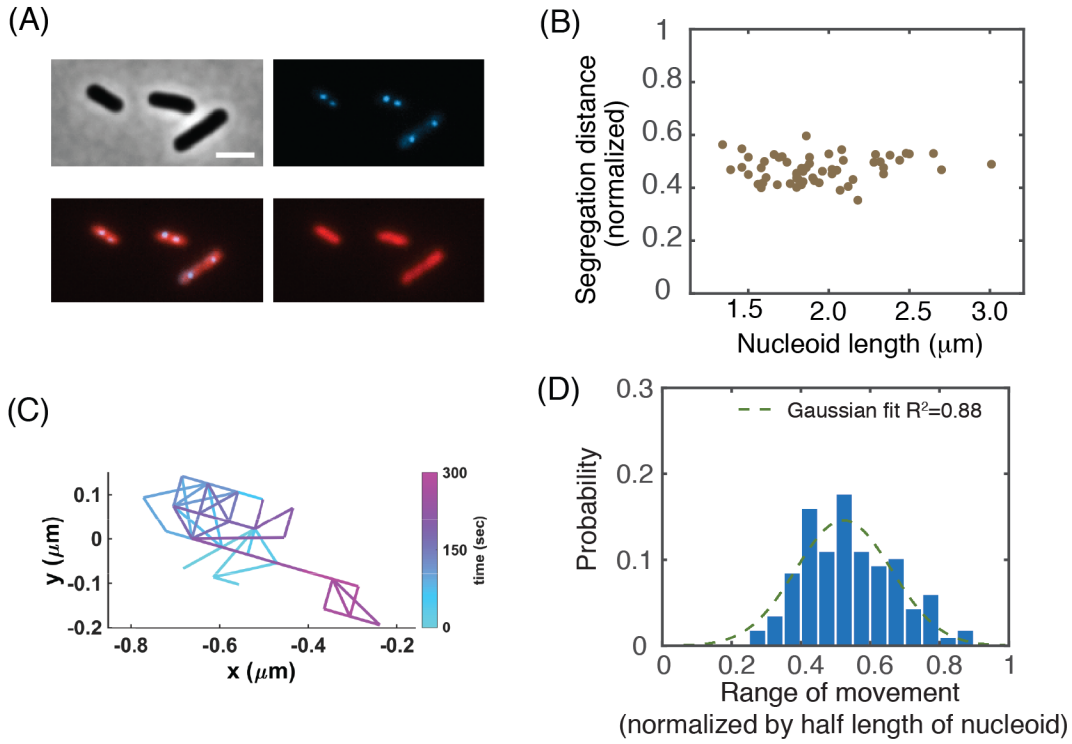
(A)
(B)
Segregation distance (normalized)
1
0.8
0.6
0.4
0.2
0
1.5
2.0
2.5
3.0
Nucleoid length (μm)
(C)
y (μm)
0.1
0
-0.1
-0.2
-0.8
-0.6
-0.4
-0.2
x (μm)
300
150
0
time (sec)
(D)
Gaussian fit R²=0.88
Probability
0.3
0.2
0.1
0
0
0.2
0.4
0.6
0.8
1
Range of movement
(normalized by half length of nucleoid)

Figure 4.

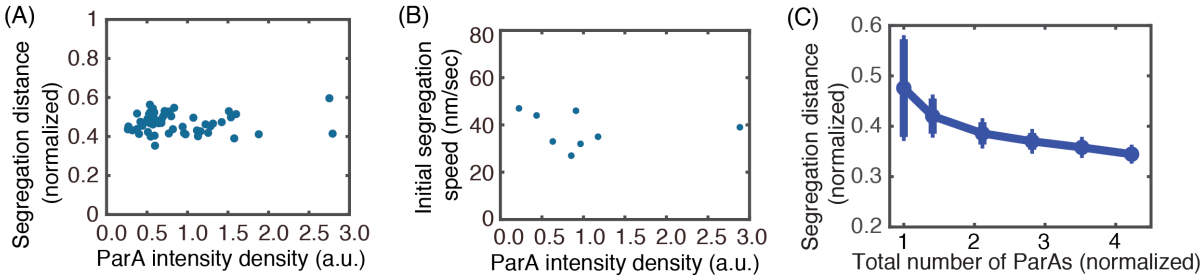
(A)
Segregation distance (normalized)
1
0.8
0.6
0.4
0.2
0
0.0 0.5 1.0 1.5 2.0 2.5 3.0
ParA intensity density (a.u.)
(B)
Initial segregation speed (nm/sec)
80
60
40
20
0
0.0 0.5 1.0 1.5 2.0 2.5 3.0
ParA intensity density (a.u.)
(C)
Segregation distance (normalized)
0.6
0.5
0.4
0.3
0.2
1 2 3 4
Total number of ParAs (normalized)

Figure 5.

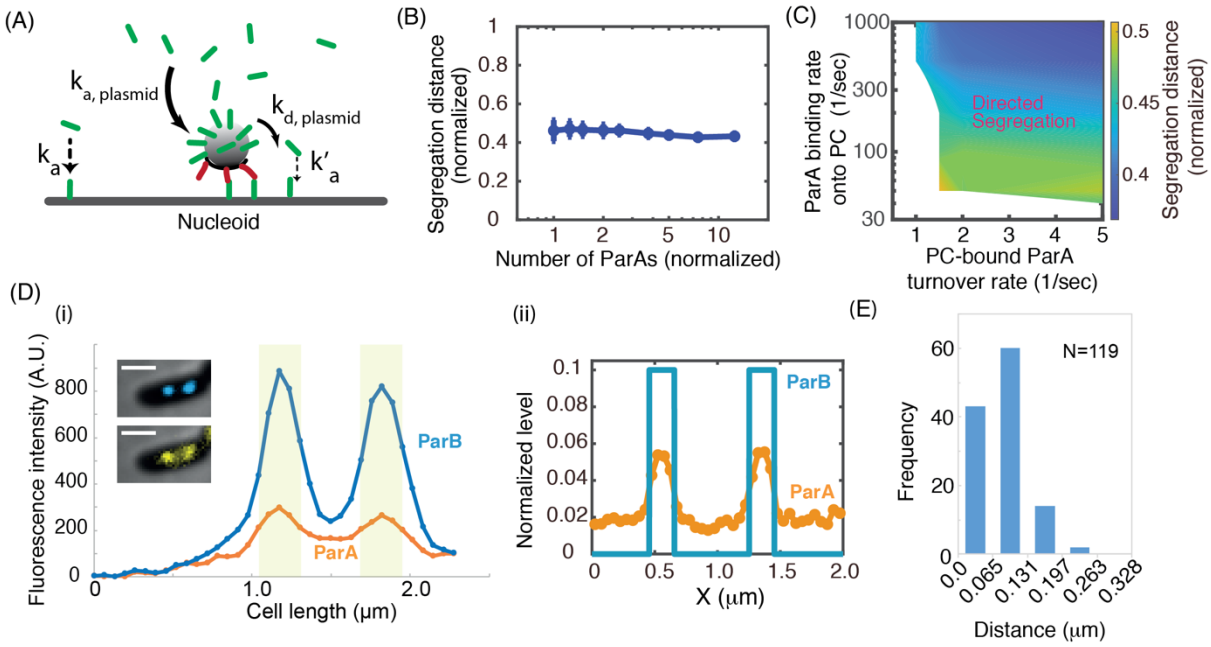
(A)
k a, plasmid
k d, plasmid
k a
k′ a
Nucleoid
(B)
Segregation distance (normalized)
Number of ParAs (normalized)
(C)
ParA binding rate onto PC (1/sec)
Directed Segregation
PC-bound ParA turnover rate (1/sec)
Segregation distance (normalized)
(D)
(i)
Fluorescence intensity (A.U.)
ParB
ParA
Cell length (μm)
(ii)
Normalized level
ParB
ParA
X (μm)
(E)
N=119
Frequency
Distance (μm)

SUPPLEMENTAL DATA

SECTION I. MODEL PARAMETER TABLE

SECTION II. SUPPLEMENTAL FIGURES

SECTION I. MODEL PARAMETER TABLE

TABLE S1. MODEL PARAMETERS

Parameter	Physical meaning	Value range	Nominal chosen value	Reference
k_{nl}	Nucleoid elongation rate	12 – 18 nm/min	12 nm/min	Our exp
k_{syn}	ParA synthesis rate	0 – 100 /min	30 /min	Estimated from (1,2) & our exp
k_{on}	Rate of ParA-ParB bond formation	10^3 – 10^4/sec	3300/sec	Estimated from (3)
k_{off}	Rate of ParA-ParB bond dissociation	~ 1.0/sec	2.0/sec	(4,5)
k_a	Rate of cytosolic ParA·ATP binding to nucleoid	0.01–2.0/sec	0.1/sec	(3-7)
k_n	Rate of $ParA^D$ conversion to ParA·ATP	~ 0.1/sec	0.1/sec	(3)
$k_{d,T}$	Rate of ParA·ATP-nucleoid dissociation	~ 0.01/sec	0.01/sec	(4,5)
$k_{d,D}$	Rate of $ParA^D$-nucleoid dissociation	~ 5.0/sec	5.0/sec	(4,5)
D_p	Diffusion constant of PC	~ 10^3 -10^4 nm^2/sec	10^4 nm^2/sec	(8)
$D_{T,N}$	Diffusion constant of ParA·ATP along nucleoid	(1-5)×10^3 nm^2/sec	1250 nm^2/sec	(5,9)
$D_{D,N}$	Diffusion constant of $ParA^D$ along nucleoid	(1-5)×10^3 nm^2/sec	1250 nm^2/sec	(5,9)
$D_{T,C}$	Diffusion constant of cytosolic ParA·ATP	~ 10^5 nm^2/sec	10^5 nm^2/sec	(5,9)
$D_{D,C}$	Diffusion constant of cytosolic $ParA^D$	10^3 nm^2/sec	10^3 nm^2/sec	(5,9)
k_S	Spring constant of ParA-ParB bond	0.2 pN/nm	0.2 pN/nm	Estimated in (10,11)
R	Radius of PC	100 nm	100 nm	(1,12)
ρ_B	ParB density on PC	~0.013/nm^2	0.013/nm^2	(1)
L_e	Equilibrium ParA-ParB bond length	50 nm	50 nm	Estimated in (11,13)
L_a	Maximal length for a newly formed bond	53 nm	53 nm	Estimated in (11,13)
X_C	Maximal bond length extension	10 nm	10 nm	Estimated in (11,13)
k_{off}^{PC}	Rate of PC-bound ParA·ATP dissociation	~ 5.0/s	5.0/sec	

k_{on}^{PC}	Rate of cytosolic ParA·ATP-PC association	10 - 1000/sec	100.0/sec	
N_C^{PC}	Upper limit of PC-localized ParA number	100-1500	500	(4,5)
P_h	Probability of PC-bound ParA re-binding to nucleoid	0 – 100%	10%	(4,5)

Note: The current model is built upon our established models (11,13), in which we have done extensive parameter sensitivity test for most of the model parameters (i.e., those in the Table 1 that are not in shade). These parameter sensitivity tests suggest that the essential features of the model – including those presented in Figs. 2 and 4 this paper – can be preserved in a broad range of model parameter space. The new ingredients in our current model pertain to the PC-localization of ParA, whose effects are characterized by the model parameters in shade in the Table 1. We have extended our parameter sensitivity tests to these parameters, the results of which are formulated as the model phase diagrams in Fig. S1 in the Section II (see below) of the Supplemental Information.

REFERENCE

1. Sanchez, A., Cattoni, Diego I., Walter, J.-C., Rech, J., Parmeggiani, A., Nollmann, M. and Bouet, J.-Y. (2015) Stochastic Self-Assembly of ParB Proteins Builds the Bacterial DNA Segregation Apparatus. *Cell Systems*, **1**, 163-173.
2. Yates, P., Lane, D. and Biek, D.P. (1999) The F plasmid centromere, sopC, is required for full repression of the sopAB operon. *Journal of Molecular Biology*, **290**, 627-638.
3. Vecchiarelli, A.G., Han, Y.-W., Tan, X., Mizuuchi, M., Ghirlando, R., Biertümpfel, C., Funnell, B.E. and Mizuuchi, K. (2010) ATP control of dynamic P1 ParA–DNA interactions: a key role for the nucleoid in plasmid partition. *Molecular Microbiology*, **78**, 78-91.
4. Hwang, L.C., Vecchiarelli, A.G., Han, Y.W., Mizuuchi, M., Harada, Y., Funnell, B.E. and Mizuuchi, K. (2013) ParA-mediated plasmid partition driven by protein pattern self-organization. *The EMBO Journal*, **32**, 1238-1249.
5. Vecchiarelli, A.G., Hwang, L.C. and Mizuuchi, K. (2013) Cell-free study of F plasmid partition provides evidence for cargo transport by a diffusion-ratchet mechanism. *Proceedings of the National Academy of Sciences*, **110**, E1390-E1397.
6. Castaing, J.-P., Bouet, J.-Y. and Lane, D. (2008) F plasmid partition depends on interaction of SopA with non-specific DNA. *Molecular Microbiology*, **70**, 1000-1011.
7. Hatano, T. and Niki, H. (2010) Partitioning of P1 plasmids by gradual distribution of the ATPase ParA. *Molecular Microbiology*, **78**, 1182-1198.
8. Vecchiarelli, A.G., Neuman, K.C. and Mizuuchi, K. (2014) A propagating ATPase gradient drives transport of surface-confined cellular cargo. *Proceedings of the National Academy of Sciences*, **111**, 4880-4885.
9. Surovtsev, Ivan V., Lim, Hoong C. and Jacobs-Wagner, C. (2016) The Slow Mobility of the ParA Partitioning Protein Underlies Its Steady-State Patterning in Caulobacter. *Biophysical Journal*, **110**, 2790-2799.
10. Bustamante, C., Smith, S.B., Liphardt, J. and Smith, D. (2000) Single-molecule studies of DNA mechanics. *Current Opinion in Structural Biology*, **10**, 279-285.

11. Hu, L., Vecchiarelli, A.G., Mizuuchi, K., Neuman, K.C. and Liu, J. (2015) Directed and persistent movement arises from mechanochemistry of the ParA/ParB system. *Proceedings of the National Academy of Sciences*, **112**, E7055-E7064.
12. Lim, H.C., Surovtsev, I.V., Beltran, B.G., Huang, F., Bewersdorf, J. and Jacobs-Wagner, C. (2014) Evidence for a DNA-relay mechanism in ParABS-mediated chromosome segregation. *eLife*, **3**, e02758.
13. Hu, L., Vecchiarelli, A.G., Mizuuchi, K., Neuman, K.C. and Liu, J. (2017) Brownian Ratchet Mechanism for Faithful Segregation of Low-Copy-Number Plasmids. *Biophysical Journal*, **112**, 1489-1502.

SECTION II. SUPPLEMENTAL FIGURES

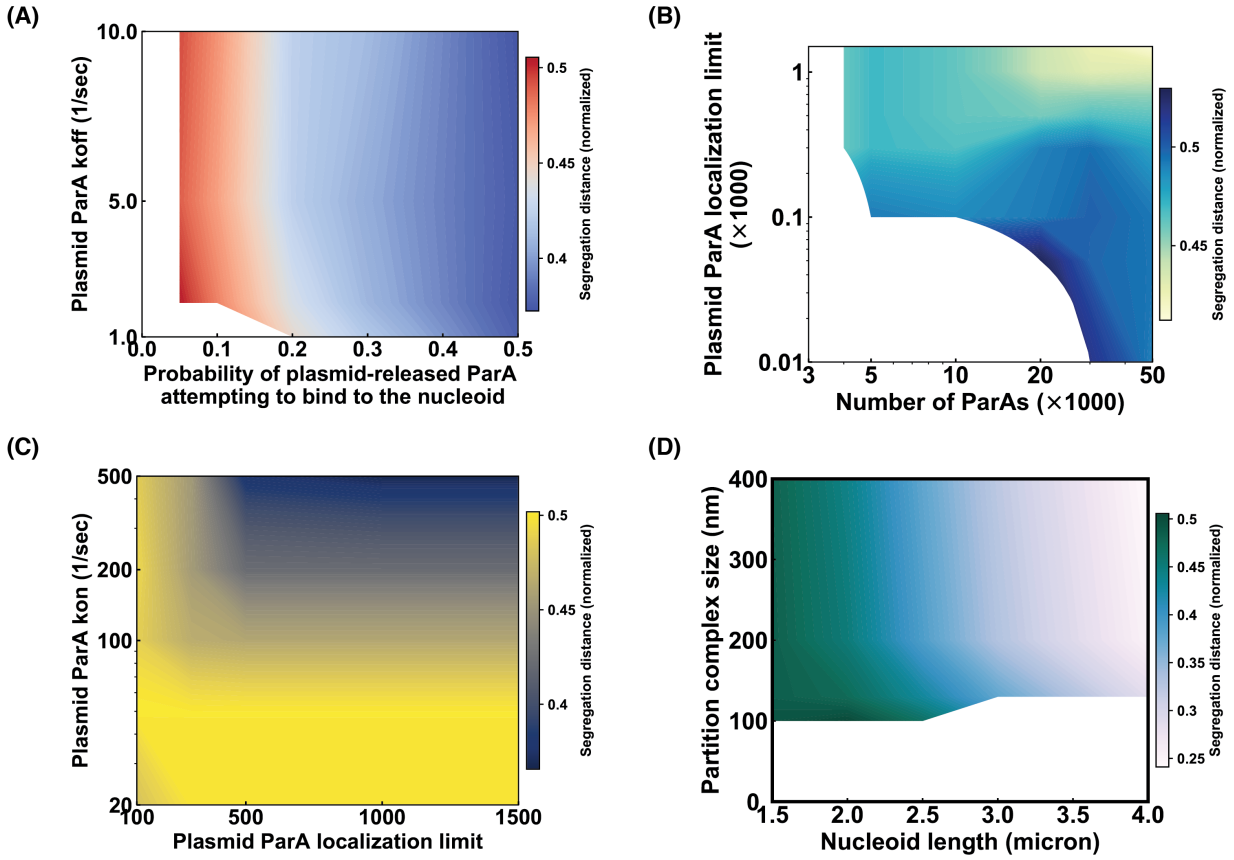

Figure S1. Model phase diagram studies of PC-ParA localization effects on PC partitioning. (A). ParA turnover rate from PC vs. percentage of PC-released ParA that binds to nucleoid. (B). Saturation level of PC-localized ParA vs. total ParA number. (C). ParA binding rate onto PC vs. Saturation level of PC-localized ParA. (D) PC size vs. nucleoid length. Here, the nucleoid length refers to the initial length of the nucleoid length in the simulation, which will elongate at the rate of 12 nm/min. For (A-D): We varied the two parameters in the respective phase diagrams, while keeping the rest of the model parameters fixed in accordance to the nominal chosen values in the Table 1. For each point in the phase diagram, we ran stochastic simulations for ≥ 36 trajectories of 10 min-dynamical evolution of the system, starting from the same initial condition and parameter set. The segregation distance reports the average value of ≥ 36 trajectories at the end of the simulation.

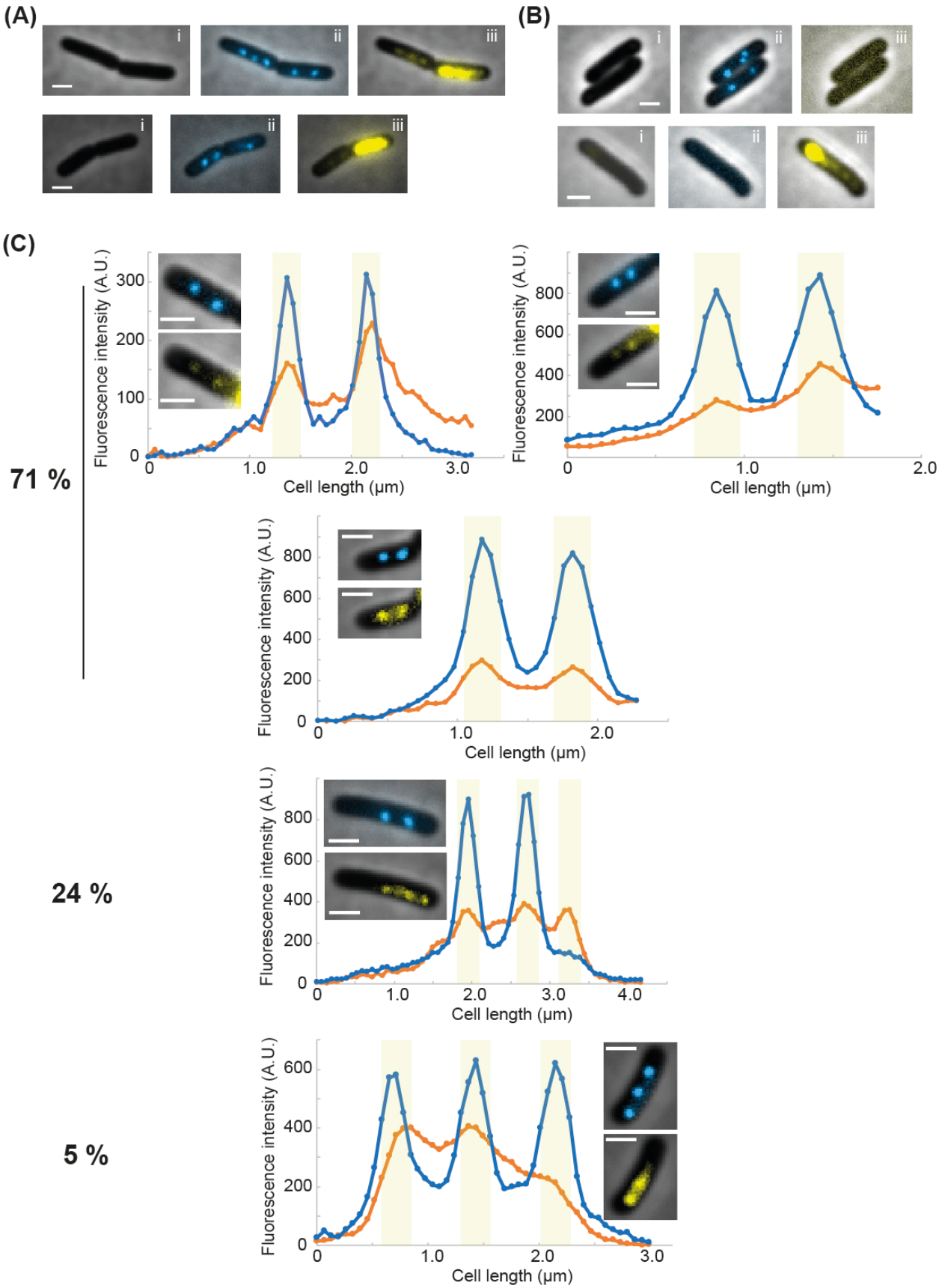

Figure S2. Co-localization of $ParA_F$ foci and partition complexes. (A) Two typical examples of asymmetric inheritance of $ParA_F$ upon cell division. Due to the oscillatory behavior of $ParA_F$, most often one cell inherits most of $ParA_F$ while the other a much smaller amount. Dividing cells are observed in phase contrast (i) and in fluorescence microcopy to observe

$ParB_F$-mTq2 (ii, blue channel) or $ParA_F$-mVenus (iii, yellow channel) in overlay with phase contrast. Cells were grown at 30°C in MGlyC. (B) Fluorescence signals are specifically detected without spreading in other channels. Strains carrying mini-F plasmids expressing either only $ParB_F$-mTurquoise (pJYB240; top) or only $ParA_F$-mVenus (pJYB243, bottom) are grown and imaged as in (A). No leaky signal from mTurquoise2 or mVenus is observed in the yellow (iii) or blue (ii) channels, respectively. (C) Line scan analyses of fluorescence intensity along cell length. Blue and orange lines correspond to the blue ($ParB_F$-mTq2) and yellow ($ParA_F$-mVenus) channels, respectively. The corresponding cell images is displayed in the graph as in (A). Over 58 cells, 41 (71%) displayed the same number of ParA and ParB foci, 14 (24%) displayed more ParA than ParB foci, and 3 (5%) displayed more ParB than ParA foci. The light green area corresponds to the limit of resolution of the microscope (i.e. 4 pixels (262 nm) around the PC peaks). Scale bar: 1 µm in all images.